Published in final edited form as:
Langmuir. 2011 June 21; 27(12): 7691–7697. doi:10.1021/la200679x.

Nanogyroids Incorporating Multivalent Lipids: Enhanced Membrane Charge Density and Pore Forming Ability for Gene Silencing

Cecília Leal[†,*], **Kai K. Ewert**[†], **Rahau S. Shirazi**[‡], **Nathan F. Bouxsein**[†], and **Cyrus R. Safinya**[†,*]

[†] Department of Physics, Department of Materials, and Molecular, Cellular & Developmental Biology Department, University of California, Santa Barbara, California 93106, United States

[‡] Department of Chemistry and Biochemistry, University of California, Santa Barbara, California 93106, United States

Abstract

The self-assembly of a custom-synthesized pentavalent cationic lipid (MVL5) and glycerol monooleate (GMO) with small interfering RNA (siRNA) results in the formation of a double-gyroid bicontinuous inverted cubic phase with co-localized lipid/siRNA domains as shown by synchrotron X-ray scattering and fluorescence microscopy. The high charge density (due to MVL5) and positive Gaussian modulus of the GMO-containing membranes confer optimal electrostatic and elastic properties for endosomal escape, enabling efficient siRNA delivery and effective, specific gene silencing.

Keywords

Multivalent lipids; Bicontinuous cubic phases; Cationic lipid–siRNA complexes; Gene silencing

INTRODUCTION

The finding that the delivery of exogenous small interfering RNA (siRNA) molecules 20–25 basepairs in length induces gene silencing[1,2] through sequence-specific cleavage of perfectly complementary messenger RNA[3–7] has stimulated a surge of research activity in the fields of functional genomics, nucleic acid (NA) therapeutics and biotechnology.[1,8–13] One of the major challenges in this field, in particular for therapeutics, is siRNA delivery. In addition to engineered viruses, cationic liposomes (CLs)[9,14,15] and other nonviral vectors such as polymers and nanoparticles[16–22] have been used to deliver siRNA to cells. CL-based nonviral NA vectors are desirable due their relative ease of production and their improved safety profile compared to viral vectors, which have on occasion exhibited serious undesirable side effects.[23–25] However, further improvement of the efficiency and specificity of target gene knockdown of nonviral siRNA vectors as well as a reduction of their cytotoxicity are required.[14]

Cecília Leal (cecilial@mrl.ucsb.edu, fax: 805 893 8797) and Cyrus R. Safinya (safinya@mrl.ucsb.edu, fax: 805 893 8797).

SUPPORTING INFORMATION

Multivalent lipid molecular structures, gene silencing activities of all Lipid–siRNA complexes discussed in the paper as a function of charge density and of neutral lipid molar fraction (for MVL2/GMO–siRNA), and experimental details. This material is available free of charge via the Internet at http://pubs.acs.org.

CL-based DNA vectors[26,27] are used in 7% of human gene delivery clinical trials.[28–30] For these and other nonviral vectors, endocytosis is the most common pathway of cell entry. We have previously shown that endosomal escape is the rate and efficiency limiting step for transfection with lamellar CL–DNA complexes of low to intermediate membrane charge density (σ_M).[31,32] In contrast, high-σ_M complexes are able to efficiently escape from endosomes via fusion of their membranes with those of the endosome. Because CL vectors typically consist of a binary mixture of cationic and neutral lipids, their membrane charge density (the average charge per membrane area) may be increased by reducing the molar fraction of neutral lipid, Φ_{NL}, as well as by increasing the headgroup charge of the cationic lipid.

Endosomal escape of the complex before it undergoes lysosomal degradation is also a crucial step in the CL-mediated delivery of siRNA. At the same time, cytotoxicity is an important concern for siRNA vectors due to the higher lipid/NA charge ratios (ρ) required for successful delivery. For mixtures of the commercially available univalent cationic lipid 2,3-dioleyloxypropyltrimethylammonium chloride (DOTAP, "1,2-dioleoyl-3-trimethylammonium-propane") with 1,2-dioleoyl-*sn*-glycero-3-phosphatidyl choline (DOPC), cytotoxicity is low at high Φ_{DOPC} (low σ_M). However, so is the gene silencing activity,[14] possibly due to inefficient endosomal escape. Interestingly, substituting DOPC with 1,2-dioleoyl-*sn*-glycero-3-phosphatidylethanolamine (DOPE), a fusogenic neutral lipid widely used in DNA delivery, gives rise to severe cytotoxicity and global inhibition of protein production.[14] A different approach to enhancing endosomal escape, based on membrane elastic theory, was more successful. Fusion of the membranes of CL-vector and endosome requires both membrane apposition and formation of membrane pores. Splay shaped membrane surfaces such as those of membrane pores have negative Gaussian curvature $C_1C_2 < 0$, where C_1 and C_2 are the principal curvatures of the membrane, and are characteristic of the membranes of inverse bicontinuous cubic phases (cf., also Figure 6). In fact, the stabilization of inverse bicontinuous cubic phases is mediated by the formation of pores.[33–35] Thus, we designed a DOTAP-based siRNA vector exhibiting the cubic phase (to favor the formation of membrane pores) by using glycerol monooleate (GMO) as the neutral lipid. GMO forms inverse bicontinuous phases in a broad composition range: the double-gyroid phase (Q_{II}^G; space group Ia3d) for low water content and the double-diamond phase (Q_{II}^D; space group Pn3m) for higher water content.[36,37] DOTAP/GMO–siRNA complexes at $\Phi_{GMO} \geq 0.75$ exhibit a double-gyroid cubic phase. These complexes show low cytotoxicity and improved gene silencing compared to DOTAP/DOPC–siRNA complexes, which are in the lamellar phase (L_α^{siRNA}).[38] While this strategy improved silencing with exclusive use of commercially available lipids, we previously also prepared effective siRNA vectors using the custom synthesized pentavalent cationic lipid MVL5[14,39] (chemical structure shown in Figure 1). Multivalent lipids such as MVL5 give access to higher membrane charge densities and have proven to be superior to monovalent lipids for DNA delivery to hard-to-transfect cells as well as for siRNA delivery.[14,40] As mentioned earlier, the high membrane charge densities accessible with these lipids can improve endosomal escape.

In the present work we aimed to harness both electrostatics and elastic membrane properties to improve the fusion of CL–siRNA complexes with endosomal membranes and thus cytoplasmic delivery of siRNA and silencing activity. We prepared CL–siRNA complexes with the inverse bicontinuous cubic structure and enhanced charge density by combining siRNA with CLs containing MVL5 and high molar fractions of GMO. These complexes achieve 80% knockdown of the targeted gene without appreciable toxicity. The combination of highly charged MVL5 with neutral GMO as a lipid favoring the cubic phase thus led to optimal conditions for endosomal escape by optimizing both the membrane charge density and the pore-forming ability. The high charge density of MVL5-containing membranes

enhances adhesion of the vector's membrane with the endosomal membrane and amplifies GMO's inherent ability to stabilize pore structures.

RESULTS AND DISCUSSION

In order to test our hypothesis that cubic-phase CL–siRNA complexes with increased σ_M would show improved endosomal escape and gene silencing, we first examined the phase behavior of siRNA complexes of mixtures of GMO with the multivalent lipids MVL2 (2+) and MVL5 (5+).[31,39] The chemical structures of these lipids are shown in Figure 1. For both MVL2 and MVL5, we found that MVL/GMO–siRNA complexes form a stable, well ordered double-gyroid cubic phase ($Q_{II}^{G,\ siRNA}$) at high contents of GMO ($\Phi_{GMO} \geq 0.85$ for MVL2, $\Phi_{GMO} \geq 0.90$ for MVL5). Figure 2A displays synchrotron small-angle X-ray scattering (SAXS) scans of isoelectric ($\rho = 1$) MVL5/GMO–siRNA complexes at $\Phi_{GMO} = 0.90$ (bottom) and $\Phi_{GMO} = 0.95$ (top). The SAXS diffraction pattern for $\Phi_{GMO} = 0.90$ is shown in Figure 2B. The large number of sharp reflections (ten) arises from a powder sample with large domains as indicated by the narrow, perfectly symmetric rings in the diffraction pattern. The peaks correspond to the reflections [*h k l*] as indicated in the figure: [211], [220], [321], [400], [420], [332], [422], [431], [440], and [543], with reciprocal lattice vectors $q/(2\pi/a) = G_{hkl}/(2\pi/a) = \sqrt{(h^2 + k^2 + l^2)} = \sqrt{6}, \sqrt{8}, \sqrt{14}, \sqrt{16}, \sqrt{20}, \sqrt{22}, \sqrt{24}, \sqrt{26}, \sqrt{32}$, and $\sqrt{50}$. These peaks can unambiguously be assigned to a body-centered gyroid cubic structure with space group Ia3d.[41] Figure 2C shows a plot of the X-ray wave-vector q versus $(h^2 + k^2 + l^2)^{1/2}$ for the Bragg reflections observed at $\Phi_{GMO} = 0.90$. The plot fits a straight line with slope $2\pi/a$, where a is the lattice spacing of the cubic phase. This lattice spacing does not vary within the studied molar fractions of GMO for MVL5/GMO–siRNA complexes and is 154 Å. Figure 2D shows SAXS scans for MVL2/GMO–siRNA complexes at $\Phi_{GMO} = 0.85$ (top), $\Phi_{GMO} = 0.80$ (middle) and at $\Phi_{GMO} = 0.75$ (bottom). At $\Phi_{GMO} = 0.85$, the characteristic pattern of the gyroid cubic $Q_{II}^{G,\ siRNA}$ phase is observed. At $\Phi_{GMO} = 0.75$, the observed reflections indicate that the complexes form the inverted hexagonal H_{II}^{siRNA} phase.[14,38] At the intermediate $\Phi_{GMO} = 0.80$, SAXS scans reveal coexistence between the $Q_{II}^{G,\ siRNA}$ and the H_{II}^{siRNA} phase. Figure 2E summarizes our SAXS experiments in a phase diagram for siRNA complexes prepared from MVL5/GMO (top), MVL2/GMO (middle), and DOTAP/GMO (bottom) lipid mixtures as a function of Φ_{GMO} at $\rho = 1$. In addition to the $Q_{II}^{G,\ siRNA}$ and the H_{II}^{siRNA} phases, the lamellar L_α^{siRNA} phase[14,38] is observed at low Φ_{GMO}. In certain regimes of Φ_{GMO}, two of the phases coexist. Notably, the phase boundaries shift systematically with headgroup size. The larger the headgroup of the cationic lipid (MVL5 > MVL2 > DOTAP), the smaller the $\Phi_{Cationic\ Lipid}$ that can successfully be incorporated into the cubic phase and thus the narrower the regime in which the $Q_{II}^{G,\ siRNA}$ phase is observed ($0.975 \leq \Phi_{GMO} \leq 0.90$ for MVL5, $0.975 \leq \Phi_{GMO} \leq 0.85$ for MVL2, $0.975 \leq \Phi_{GMO} \leq 0.75$ for DOTAP). The regime in which the H_{II}^{siRNA} phase is observed behaves in a similar fashion. In fact, this phase was not observed for MVL5/GMO–siRNA complexes, meaning that it either does not form in this system or only in a very narrow composition range (we mapped the phase diagram as a function of Φ_{GMO} in steps of 0.05). These trends are easily understood because the larger headgroups of the multivalent lipids favor positive membrane curvature while both the $Q_{II}^{G,\ siRNA}$ and the H_{II}^{siRNA} phase consist of surfaces where one of the principal curvatures C_1 and C_2 is negative. In fact, to the best of our knowledge, cubic lipid phases containing multivalent charged lipids have not been previously reported. Despite the reduced range of Φ_{GMO} for which the cubic phase is observed, substituting monovalent DOTAP with pentavalent MVL5 approximately doubles the maximum achievable membrane charge density (cf., Figure S2 in the Supporting Information).

Figure 3A shows a schematic representation of the unit cell of the bicontinuous gyroid cubic phase of CL–siRNA complexes ($Q_{II}^{G,\ siRNA}$). The $Q_{II}^{G,\ siRNA}$ phase is comprised of a

bilayer surface separating two continuous, independent, and intertwined water nanochannels (blue and orange) that contain the siRNA. For clarity, the bilayer is not shown in its entire thickness in Figure 3A. Instead, it is represented by an imaginary surface (grey) at the center of the membrane as indicated in the enlarged inset. Note the abundance of pore-like membrane structures in the unit cell. The bilayer is comprised mostly of GMO, containing no more than 10 mol% MLV5. Figure 3B shows the morphology of MVL5/GMO–siRNA lipid complexes in the cubic phase regime ($\Phi_{GMO} = 0.90$, $\rho = 1$) as investigated by differential-interference-contrast (Figure 3B, left panel) and fluorescence optical microscopy (Figure 3B, middle panels). The complexes consist of globular aggregates which display a perfect overlap of lipid and siRNA distributions in the two fluorescence modes (Figure 3B, right panel). This colocalization of lipid and siRNA domains unambiguously demonstrates that the bicontinuous cubic phase incorporates the siRNA molecules. In addition, UV absorption measurements indicate that less than 2% of the total siRNA concentration remain in the supernatant after complex formation. The efficient silencing mediated by the MVL5/GMO–siRNA complexes (see below) also provides evidence that siRNA is incorporated in the cubic phase.

The gene silencing efficiency (a measure of post-transcriptional knockdown of the gene targeted by the transferred exogenous siRNA) of MVL/GMO–siRNA complexes was assessed in mouse fibroblast L-cells at varied charge ratio (ρ) and neutral lipid content (Φ_{NL}) and thus complex phase. For comparison, we also measured the silencing efficiency of MVL5/DOPC–siRNA complexes[14] and DOTAP/GMO–siRNA complexes.[38] The cells were pre-transfected with two plasmids encoding distinct luciferase genes (*firefly* (FF) and *renilla* (RL)). After this step, the cells were treated with CL complexes of an siRNA that targets solely the FF gene. Gene silencing was assessed by measuring both the FF and RL expression levels with a dual luciferase assay. This allowed simultaneous measurement of total knockdown (K_T, comprising specific *and* nonspecific knockdown) and nonspecific knockdown (K_{NS}) as knockdown of the FF and RL expression, respectively.[14]

An optimal gene silencing vector would show a K_T approaching unity at a K_{NS} of nearly zero. We only discuss the data for MVL5/GMO–siRNA complexes below because MVL2/GMO–siRNA complexes exhibited pronounced nonspecific silencing (see Figure S1 in the Supporting Information). This is in line with other experiments in which we have found divalent cationic lipids to be more toxic than other multivalent lipids. The origin of this phenomenon is still under investigation.

Figure 4A shows the total and nonspecific knockdown as a function of mole fraction of neutral lipid, Φ_{NL}, at fixed $\rho = 10$ (shown before to be effective in gene silencing experiments with MVL5[14]). Filled and open symbols indicate K_T and K_{NS}, respectively, while symbol shape indicates the phase of the complexes as cubic ($Q_{II}^{G,\ siRNA}$, squares), inverted hexagonal (H_{II}^{siRNA}, triangles) or lamellar (L_{α}^{siRNA}, circles). For the entire range of Φ_{NL} investigated ($0.95 \geq \Phi_{NL} \geq 0.05$), MVL5/GMO–siRNA complexes achieve high total gene knockdown ($K_T \approx 0.8$, 0.89 to 0.77). The total knockdown induced by DOTAP/GMO–siRNA complexes also hardly varies with Φ_{NL} but is significantly lower ($K_T \approx 0.7$, 0.74 to 0.60). For MVL5/DOPC–siRNA complexes, K_T increases with Φ_{NL} from $K_T < 0.4$ at $\Phi_{NL} = 0.95$ to values comparable with the DOTAP/GMO system at lower Φ_{NL} ($\Phi_{NL} < 0.5$). Finally, at very low Φ_{NL} ($\Phi_{NL} \leq 0.1$, i.e. ≥ 90 mol% MVL5 in the membrane), DOPC-containing siRNA complexes of MVL5 achieve K_T similar to that of GMO-containing complexes. The nonspecific silencing is insignificant for all systems at this ρ. The fact that MVL5/GMO–siRNA complexes exhibit high K_T at low K_{NS} over the entire range of Φ_{NL} makes them the most desirable system for future applications, where the required addition of other lipid components (such as PEG-lipids) changes Φ_{NL}. A few other points are also worth noting. The K_T for MVL5/GMO–siRNA complexes is high at high Φ_{NL} even if the

complexes are lamellar. This is not simply due to an increased membrane charge density because of the small headgroup size of GMO (see below and Figure S2 in the Supporting Information). Furthermore, and unlike the transfection efficiency of MVL5-containing CL–DNA complexes,[31] K_T does not decrease at low Φ_{NL} (high σ_M). This likely reflects differences in the delivery mechanism, which might stem from the shorter length of the siRNA cargo and the resulting reduced complex stability or from the fact that siRNA does not need to be transferred to the nucleus to unfold its activity.

Figure S2 in the Supporting Information shows the data of Figure 4A plotted against the σ_M. We calculated the membrane charge densityas $\sigma_M = eZN_{CL}/(N_{CL}A_{CL} + N_{NL}A_{NL}) = eZ\Phi_{CL}/(\Phi_{CL}A_{CL} + \Phi_{NL}A_{NL})$ where A_{CL} and A_{NL} are the headgroup areas of the cationic and the neutral lipid, respectively, e is the elementary charge, and Z the valency of the cationic lipid. We used $Z_{DOTAP} = 1$, $Z_{MVL5} = 4.5 \pm 0.1$, $A_{DOPC} = A_{DOTAP} = 72$ Å^2, $A_{MVL5} = 166$ Å^2,[31] and $A_{GMO} = 33$ Å^2.[42,43] Switching to a cationic lipid of higher valency (e.g. MVL5 in place of DOTAP) or to a neutral lipid with smaller headgroup (e.g. GMO in place of DOPC) are both strategies to increase σ_M at a given Φ_{NL}. For lamellar DNA complexes, weak electrostatic attraction between the complex and the endosomal membrane at low σ_M coincides with poor transfection efficiency (TE) due to endosomal entrapment of the complexes.[31,32] Thus, TE increases exponentially with σ_M to a maximum and then drops again, possibly due to inhibited release of DNA from the high-σ_M complexes. Somewhat similarly, the silencing efficiency (measured here as K_T), of MVL5/DOPC–siRNA complexes increases with σ_M but does not drop at very high σ_M. Figure S2 further shows that the increased silencing efficiency of MVL5/GMO–siRNA complexes (compared to MVL5/DOPC–siRNA complexes) in the regime where both complexes are lamellar is not simply due to an increase in σ_M. Finally, the plot shows that despite the narrower range of Φ_{NL} in which $Q_{II}^{G,\,siRNA}$ complexes form in the MVL5/GMO system, the maximum charge density of cubic MVL5/GMO–siRNA complexes is about twice that of DOTAP/GMO–RNA complexes.

Figure 4B shows the total and nonspecific knockdown for the same lipid combinations as Figure 4A, but as a function of the charge ratio ρ at fixed siRNA concentration and $\Phi_{NL} = 0.90$. At this Φ_{NL}, all GMO-containing complexes are in the cubic phase and the DOPC-containing complexes are in the lamellar phase. For all lipid systems, K_T initially steeply increases with ρ and then saturates. Nonspecific silencing remains reasonably low for all systems ($0 \le K_{NS} \le 0.23$) up to $\rho = 15$. At higher ρ, K_{NS} rapidly increases (arrow) and eventually accounts for most ($\rho = 30$) or even all of K_{NS} ($\rho = 50$). This highlights the importance of measuring both K_T and K_{NS}. Over the entire range of ρ, MVL5-containing complexes in the cubic $Q_{II}^{G,\,siRNA}$ phase (blue filled) exhibit the highest total gene knockdown of the three systems, followed by DOTAP/GMO–siRNA complexes (at values of ρ where K_{NS} is low).

The source of the observed high K_{NS} at high charge ratios typically is cytotoxicity of the CL vector.[14] Thus, the evaluation of nonviral siRNA delivery vectors must include a careful assessment of this parameter. We measured cytotoxicity both as a reduction in cell viability and as compromised plasma membrane integrity, employing a tetrazolium salt-based assay[44] and a standard assay measuring extracellular levels of lactate dehydrogenase, respectively. The latter is particularly important for lipid vectors with fusogenic capabilities such as the cubic $Q_{II}^{G,\,siRNA}$ phase. Figures 5A and 5B plot the percentage of viable cells and of cells with unperturbed plasma membranes, respectively, as a function of total lipid concentration at $\Phi_{NL} = 0.90$ (as in Figure 4B) for MVL5/GMO and MVL5/DOPC lipid mixtures with and without siRNA. The MVL5/GMO–siRNA complexes (red squares) exhibit the cubic phase while the MVL5/DOPC–siRNA complexes (red circles) are lamellar. Because siRNA concentration and total sample volume are kept constant, the total lipid concentration is also

a measure of the charge ratio ρ (displayed in red in the top x-axis). Remarkably, all systems (including DOTAP/GMO–siRNA complexes[38]) display the same general behavior, showing an onset of cytotoxicity at lipid concentrations of 0.15 mM (ρ = 20) that correlates well with the onset of nonspecific silencing (cf., arrow in Figure 4B). Thus, despite its high silencing efficiency that we attribute to enhanced fusion with endosomal membranes, the MVL5-based cubic phase (existing exclusively at high GMO contents) is no more toxic than the lamellar phase. This means that the intrinsic ability of CL–siRNA cubic phase particles to promote membrane fusion selectively affects the endosomal membrane but not the plasma membrane. Two factors likely contribute to this: (i) the external cellular membrane is protected by the glycocalix, and (ii) confinement of the cubic CL-siRNA complexes within the small endosomal compartments increases the number of inter-membrane collisions (required for fusion) over that occurring between the plasma membrane and CL–siRNA complexes outside of the cell. The fact that cytotoxicity is independent of the presence of siRNA demonstrates that the main source of cytotoxicity is the lipid component. It is therefore desirable to develop CL–siRNA complexes that exhibit efficient silencing at low ρ. As a comparison of the MVL5-containing vectors in Figure 4B illustrates, MVL5/GMO–siRNA complexes achieve this objective by employing a physico-chemical approach, increasing pore-forming ability (and also σ_M) by exchanging the neutral lipid.

Biotechnology applications based on siRNA are currently assuming a leading role in areas that extend beyond functional genomics, with therapeutics being the most exciting and promising field. The formulation of efficient siRNA delivery vectors with low toxicity is the enabling step for any major discovery in siRNA-based gene silencing technology and required for viable therapeutics. In the present work, we have presented an optimal lipid carrier of siRNA that enables highly specific and efficient gene silencing with virtually no adverse effects on cell viability and plasma membrane integrity. This was achieved by optimizing specific physico-chemical characteristics that overcome the major barrier of endosomal entrapment. The preference of GMO for cubic phases increases the ability of the lipid membranes to form pores, while the pentavalent MVL5 increases their charge density. This is illustrated in Figure 6 which shows a schematic representation of the complexes' mechanism of action. The main route for cell entry is endocytosis (II), after which the CL–siRNA complex is incorporated in the endosome (III). It needs to escape the endosome (IV) to avoid lysosomal degradation and release its siRNA cargo into the cytoplasm. This requires fusion of the membranes of the CL–siRNA complex and the endosome (IV). The high membrane charge density of the complex (due to MVL5) increases the electrostatic attraction to the negatively charged endosomal membrane (III), thus promoting membrane apposition. The elastic properties of the cubic phase, specifically the positive Gaussian modulus, $\kappa_G > 0$, favor formation of saddle-splay membrane structures with negative Gaussian curvature ($C_1C_2 < 0$). Therefore, once close contact between the membranes is established, the membranes of the bicontinuous cubic phase likely facilitate the formation of pores and fusion with the endosomal membrane, which also involves structures with negative Gaussian curvature (cf., Figure 6).[38] Overall, these processes promote the fusion of the outer membrane of CL–siRNA complexes and the adjacent endosomal membrane, resulting in endosomal escape and thus efficient cytoplasmic delivery of siRNA. In this way, our results also indirectly confirm the importance of the barrier of endosomal escape for siRNA delivery and gene silencing with CL–siRNA complexes and validate the above-mentioned strategies to overcome it.

EXPERIMENTAL SECTION

MVL2 and MVL5 were prepared as described[31,39] The complex preparation and experimental methods used have been described elsewhere[14,38] and are provided in the Supporting Information.

Supplementary Material

Refer to Web version on PubMed Central for supplementary material.

Acknowledgments

We acknowledge support by NIH GM-59288 (structure–biological activity studies), DOE-BES grant number DOE-DE-FG02-06ER46314 (liposome–nucleic acid cubic phase structure), and NSF DMR-0803103 (phase behavior). Cecília Leal was funded by the Swedish Research Council (VR) and in part by DOE-BES. The X-ray diffraction work was carried out at the Stanford Synchrotron Radiation Lightsource (SSRL) beam line 4.2. CRS acknowledges useful discussions with KAIST Faculty where he has a WCU (World Class University) Visiting Professor of Physics appointment supported by the National Research Foundation of Korea funded by the Ministry of Education, Science and Technology No. R33-2008-000-10163-0.

References

1. Elbashir SM, Harborth J, Lendeckel W, Yalcin A, Weber K, Tuschl T. Nature. 2001; 411:494. [PubMed: 11373684]
2. Caplen NJ, Parrish S, Imani F, Fire A, Morgan RA. Proc Natl Acad Sci USA. 2001; 98:9742. [PubMed: 11481446]
3. Fire A, Xu SQ, Montgomery MK, Kostas SA, Driver SE, Mello CC. Nature. 1998; 391:806. [PubMed: 9486653]
4. Hammond SM, Caudy AA, Hannon GJ. Nature Rev Genet. 2001; 2:110. [PubMed: 11253050]
5. Jorgensen R, Cluster PD, English J, Que Q, Napoli CA. Plant Mol Biol. 1996; 31:957. [PubMed: 8843939]
6. Napoli CA, Lemieux C, Jorgensen R. Plant Cell. 1990; 2:279. [PubMed: 12354959]
7. Cogoni C, Macino G. Curr Opin Genet Dev. 2000; 10:638. [PubMed: 11088014]
8. Caplen NJ. Expert Opin Biol Ther. 2003; 3:575. [PubMed: 12831363]
9. Hannon GJ, Rossi JJ. Nature. 2004; 431:371. [PubMed: 15372045]
10. Karagiannis TC, El-Osta A. Cancer Gene Ther. 2005; 12:787. [PubMed: 15891770]
11. Martinez LA, Naguibneva I, Lehrmann H, Vervisch A, Tchenio T, Lozano G, Harel-Bellan A. Proc Natl Acad Sci USA. 2002; 99:14849. [PubMed: 12403821]
12. McManus MT, Sharp PA. Nature Rev Genet. 2002; 3:737. [PubMed: 12360232]
13. Sioud M. Trends Pharm Sci. 2004; 25:22. [PubMed: 14723975]
14. Bouxsein NF, McAllister CS, Ewert K, Samuel CE, Safinya CR. Biochemistry. 2007; 46:4785. [PubMed: 17391006]
15. Santel A, Aleku M, Keil O, Endruschat J, Esche V, Fisch G, Dames S, Löffler K, Fechtner M, Arnold W, Giese K, Klippel A, Kaufmann J. Gene Therapy. 2006; 2006:1222. [PubMed: 16625243]
16. Braun GB, Pallaoro A, Wu G, Missirlis D, Zasadzinski JA, Tirrell M, Reich NO. ACS Nano. 2009; 3:2007. [PubMed: 19527019]
17. Chu TC, Twu KY, Ellington AD, Levy M. Nucleic Acid Res. 2006; 34:e73. [PubMed: 16740739]
18. del Pino P, Munoz-Javier A, Vlaskou D, Gil PR, Plank C, Parak WJ. Nanoletters. 2010; 10:3914.
19. Giljohann DA, Seferos DS, Prigodich AE, Patel PC, Mirkin CA. J Am Chem Soc. 2009; 131:2072. [PubMed: 19170493]
20. Schaffert D, Wagner W. Gene Ther. 2008; 15:1131. [PubMed: 18528432]
21. Simeoni F, Morris MC, Heitz F, Gilles D. Nucleic Acid Res. 2003; 31:2717. [PubMed: 12771197]
22. Zhou J, Wu J, Hafdi N, Behr JP, Erbacherc P, Peng L. Chem Commun. 2006:2362.
23. Hacein-Bey-Abina S, Garrigue A, Wang GP, Soulier J, Lim A, Morillon E, Clappier E, Caccavelli L, Delabesse E, Beldjord K, Asnafi V, Macintyre E, Dal Cortivo L, Radford I, Brousse N, Sigaux F, Moshous D, Hauer J, Borkhardt A, Belohradsky BH, Wintergerst U, Velez MC, Leiva L, Sorensen R, Wulffraat N, Blanche S, Bushman FD, Fischer A, Cavazzana-Calvo M. J Clin Invest. 2008; 118:3132. [PubMed: 18688285]
24. Thomas CE, Ehrhardt A, Kay MA. Nature Rev Genet. 2003; 4:346. [PubMed: 12728277]

25. Williams DA, Baum C. Science. 2003; 302:400. [PubMed: 14563994]
26. Felgner PL, Gadek TR, Holm M, Roman R, Chan HW, Wenz M, Northrop JP, Ringold GM, Danielsson M. Proc Natl Acad Sci USA. 1987; 84:7413. [PubMed: 2823261]
27. Huang, L.; Hung, M-C.; Wagner, E. Advances in Genetics, Vol 53: Non-Viral Vectors for Gene Therapy. 2. Elsevier; San Diego: 2005.
28. Edelstein ML, Abedi MR, Wixon J. J Gene Med. 2007; 9:833. [PubMed: 17721874]
29. Edelstein ML, Abedi MR, Wixon J, Edelstein RM. J Gene Med. 2004; 6:597. [PubMed: 15170730]
30. http://www.wiley.com/legacy/wileychi/genmed/clinical.
31. Ahmad A, Evans HM, Ewert K, George CX, Samuel CE, Safinya CR. J Gene Med. 2005; 7:739. [PubMed: 15685706]
32. Lin AJ, Slack NL, Ahmad A, George CX, Samuel CE, Safinya CR. Biophys J. 2003; 84:3307. [PubMed: 12719260]
33. Porte G. J Phys Condens Matter. 1992; 4:8649.
34. Siegel DP, Epand RM. Biophys J. 1997; 73:3089. [PubMed: 9414222]
35. Yang L, Huang HW. Science. 2002; 297:1877. [PubMed: 12228719]
36. Briggs J, Chung H, Caffrey M. J Phys II France. 1996; 6:723.
37. Larsson K. Nature. 1983; 304:664.
38. Leal C, Bouxsein N, Ewert K, Safinya CR. J Am Chem Soc. 2010; 132:16841. [PubMed: 21028803]
39. Ewert K, Ahmad A, Evans HM, Schmidt HW, Safinya CR. J Med Chem. 2002; 45:5023. [PubMed: 12408712]
40. Ewert K, Evans HM, Zidovska A, Bouxsein NF, Ahmad A, Safinya CR. J Am Chem Soc. 2006; 128:3996.
41. Hahn, T. Space-group symmetry. 3. Vol. A. Kluwer Academic: Dordrecht/Boston/London; 1992. International tables for crystallography. revised edition
42. Chung H, Caffrey M. Biophys J. 1994; 66:377. [PubMed: 8161691]
43. Mariani P, Rustichelli F, Saturni L, Cordone L. Eur Biophys J. 1999; 28:294.
44. Cory AH, Owen TC, Barltrop JA, Cory JG. Cancer Comm. 1991; 3:207.
45. Wohlgemuth M, Yufa N, Hoffman J, Thomas EL. Macromolecules. 2001; 34:6083.

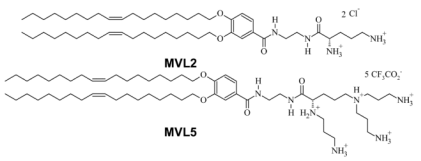

Figure 1.
Chemical structure of the custom-synthesized multivalent lipids used in this work.[39]

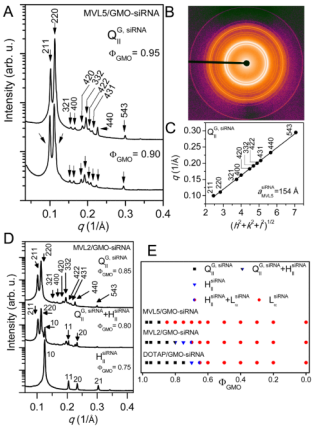

Figure 2.

Synchrotron small-angle X-ray scattering (SAXS) data and phase diagram for cationic lipid/GMO–siRNA complexes. A) SAXS data for MVL5/GMO–siRNA complexes at Φ_{GMO} = 0.95 (top), and at Φ_{GMO} = 0.90 (bottom). The large number of observed peaks can unambiguously be assigned to a body centered gyroid cubic structure with space group Ia3d, termed $Q_{II}^{G,\ siRNA}$,[38] (cf., also Figure 2). B) SAXS diffraction pattern acquired for MVL5/GMO–siRNA complexes at Φ_{GMO} = 0.90. The bright and narrow symmetric rings indicate the presence of a perfect powder sample with large domains. C) Plot of the wave-vector q versus $(h^2 + k^2 + l^2)^{1/2}$ showing the expected straight line (with slope $2\pi/a$, where a = 154 Å is the unit cell dimension) for cubic MVL5/GMO–siRNA complexes at Φ_{GMO} = 0.90. The data points correspond to reflections shown in part A. D) SAXS data for MVL2/GMO–siRNA complexes at Φ_{GMO} = 0.85 (top), Φ_{GMO} = 0.80 (middle) and at Φ_{GMO} = 0.75 (bottom). At Φ_{GMO} = 0.85, the characteristic pattern of the Ia3d cubic $Q_{II}^{G,\ siRNA}$ phase is observed. At Φ_{GMO} = 0.80, SAXS scans reveal a coexistence between the $Q_{II}^{G,\ siRNA}$ and the inverted hexagonal H_{II}^{siRNA} phase.[14,38] At Φ_{GMO} = 0.75, only the reflections from the H_{II}^{siRNA} phase are present. E) Phase diagram for siRNA complexes of MVL5/GMO (top), MVL2/GMO (middle), and DOTAP/GMO (bottom) lipid mixtures as a function of Φ_{GMO} at ρ = 1. Three different phases (and coexistence between them) are observed: $Q_{II}^{G,\ siRNA}$, H_{II}^{siRNA}, and the lamellar L_{α}^{siRNA} phase[14,38] The phase boundaries shift systematically with headgroup size (see discussion in the text).

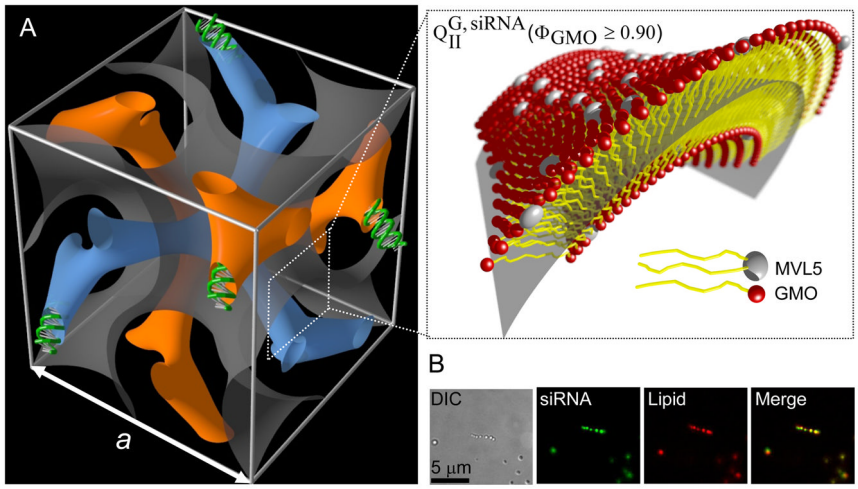

Figure 3.

A) Schematic depiction of a unit cell of MVL5/GMO–siRNA complexes in the double-gyroid (Ia3d) cubic phase, $Q_{II}^{G, siRNA}$, obtained for MVL5/GMO–siRNA complexes at $0.90 \leq \Phi_{GMO} \leq 0.975$. The surfaces were generated using the level-set equations[45] A lipid bilayer surface separates two independent, continuous water channels (blue and orange) containing the siRNA. For clarity, the bilayer is not shown in its entire thickness but represented by an imaginary surface (grey) corresponding to a thin layer in the membrane midplane as indicated in the enlarged inset. The majority of the membrane is comprised of GMO (red), with no more than 10 mol% of pentavalent cationic MVL5 (white, note the larger headgroup). B) Optical microscopy images of MVL5/GMO–siRNA complexes in the cubic phase region ($\Phi_{GMO} = 0.90$) at charge ratio $\rho = 1$. Complexes were viewed in differential-interference-contrast mode (left), siRNA fluorescence mode (second panel) and lipid fluorescent mode (third panel). As evident from the merged image (right panel), lipids and siRNA are completely co-localized in the globular CL–siRNA lipid complexes.

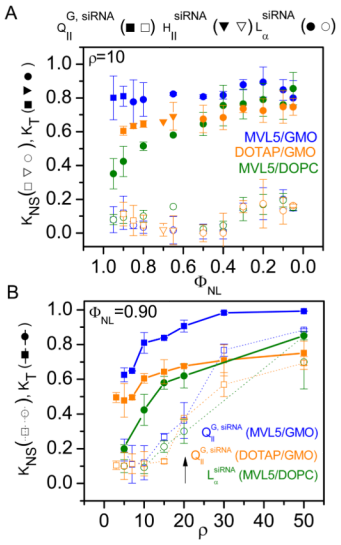

Figure 4.

Total (K_T, filled symbols) and nonspecific (K_{NS}, open symbols) gene knockdown for siRNA complexes prepared from MVL5/GMO (blue), MVL5/DOPC (orange) and DOTAP/GMO lipid mixtures. A) K_T and K_{NS} as a function of mole fraction of neutral lipid (Φ_{NL}) at fixed ρ = 10. B) K_T and K_{NS} as a function of ρ at fixed Φ_{NL} = 0.90. MVL5/GMO–siRNA complexes show improved, high, and specific silencing. In the regime where they exhibit the gyroid cubic $Q_{II}^{G, siRNA}$ phase, the improvement over MVL5/DOPC–siRNA complexes is biggest. The arrow indicates the onset of nonspecific silencing at ρ = 20.

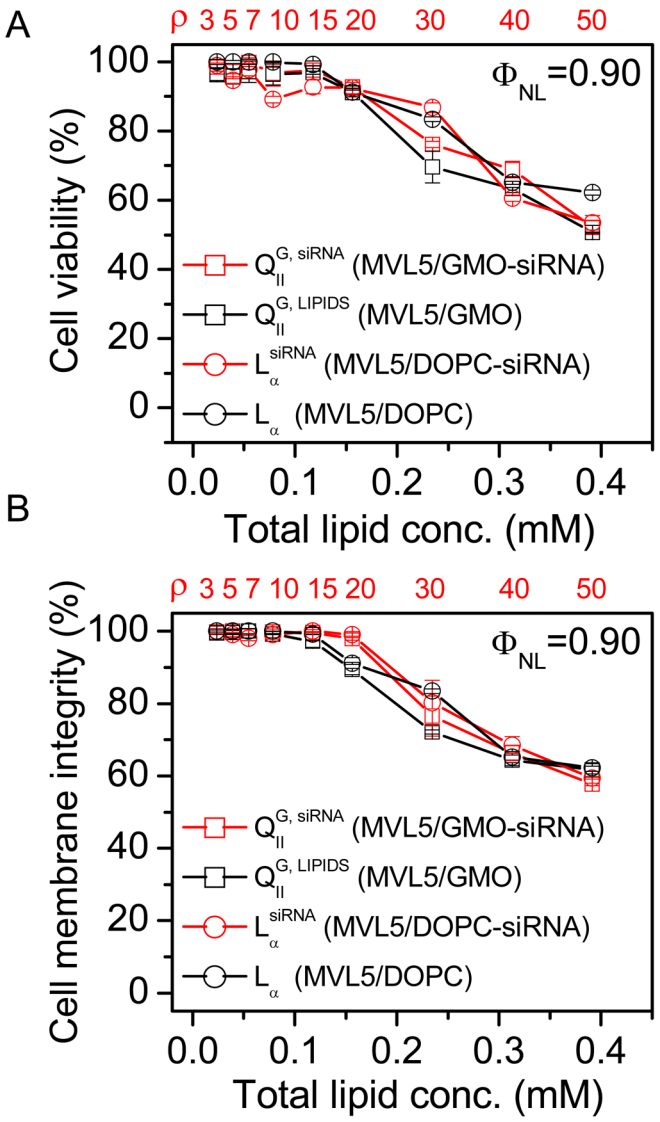

Figure 5.

Cytotoxicity of MVL5-based CL–siRNA complexes at Φ_{NL} = 0.90 (as in Figure 3B). A) Cell viability and B) membrane integrity as a function of total lipid concentration for cells incubated with $Q_{II}^{G,\ siRNA}$ MVL5/GMO–siRNA complexes (red squares) and L_{α}^{siRNA} MVL5/DOPC–siRNA complexes (red circles). Also shown is the cytotoxicity of the corresponding lipid mixtures without siRNA (black). The top x-axis indicates the corresponding charge ratio, ρ, for samples containing siRNA. For both cytotoxicity assays the data is unaffected by the phase of the complexes as well as the presence or absence of siRNA. Both cell viability and membrane integrity remain around above 90% up to high lipid concentrations, and the onset of toxicity corresponds directly to the observed increase in K_{NS}.

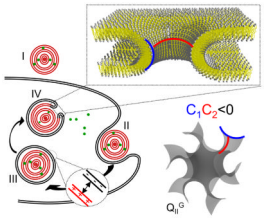

Figure 6.
Schematic illustration of the siRNA delivery pathway of CL–siRNA complexes. Cell attachment (I) is followed by endocytosis (II). Complexes in the endosome (III) need to escape into the cytoplasm to deliver their siRNA cargo. This is enabled by fusion of the membranes of the complex with the endosomal membrane, which results in pore formation (IV). The fusion process is aided by electrostatic attraction of endosomal and complex membranes (III) and the propensity of cubic phase-forming lipids to stabilize pore structures with negative Gaussian curvature. In the enlarged view of a pore and the schematic of the membrane structure of the gyroid cubic phase, blue and red lines indicate positive and negative curvature, respectively.